Monthly Notices of the ROYAL ASTRONOMICAL SOCIETY

MNRAS **537,** 1220–1231 (2025) https://doi.org/10.1093/mnras/staf072
Advance Access publication 2025 January 15

The formation of mini-AGN discs around IMBHs and their dynamical implications

Mor Rozner [1,2,3,4★] Alessandro A. Trani [5] Johan Samsing [5] and Hagai B. Perets [2,6]

[1]*Institute of Astronomy, University of Cambridge, Madingley Road, Cambridge CB3 0HA, UK*
[2]*Technion – Israel Institute of Technology, Haifa 3200002, Israel*
[3]*Gonville & Caius College, Trinity Street, Cambridge CB2 1TA, UK*
[4]*Institute for Advanced Study, Einstein Drive, Princeton, NJ 08540, USA*
[5]*Niels Bohr International Academy, Niels Bohr Institute, Blegdamsvej 17, DK-2100, Copenhagen, Denmark*
[6]*Astrophysics Research Center of the Open University (ARCO), The Open University of Israel, PO Box 808, Raa'nana 4353701, Israel*

Accepted 2025 January 9. Received 2024 December 20; in original form 2024 September 27

ABSTRACT

This study explores the formation and implications of mini-active galactic nucleus (mAGN) discs around intermediate-mass black holes (IMBHs) embedded in gas-rich globular/nuclear clusters (GCs). We examine the parameter space for stable mAGN discs, considering the influence of IMBH mass, disc radius, and gas density on disc stability. The dynamics of stars and black holes within the mAGN disc are modelled, with a focus on gas-induced migration and gas dynamical friction. These dynamical processes can lead to several potentially observable phenomena, including the enhancement of gravitational wave mergers (particularly intermediate-mass ratio inspirals and extreme-mass ratio inspirals), and the occurrence of milli/centi-tidal disruption events with unique observational signatures. We find that gas hardening can significantly accelerate the inspiral of binaries within the disc, potentially leading to a frequency shift in the emitted gravitational waves. Additionally, we explore the possibility of forming accreting IMBH systems from captured binaries within the mAGN disc, potentially resulting in the formation of ultraluminous X-ray sources. The observational implications of such accreting systems, including X-ray emission, optical signatures, and transient phenomena, are discussed. Furthermore, we investigate the possibility of large-scale jets emanating from gas-embedded IMBHs in GCs. While several caveats and uncertainties exist, our work highlights the potential for mAGN discs to provide unique insights into IMBH demographics, accretion physics, and the dynamics of GCs.

Key words: accretion, accretion discs – gravitational waves – black hole mergers – transients: tidal disruption events.

1 INTRODUCTION

Intermediate-mass black holes (IMBHs), with masses of 10^2–10^5 $M_\odot$, occupy a unique range in the black hole (BH) mass spectrum. While stellar-mass BHs (SBHs) and supermassive BHs (SMBHs) are well established through numerous observations, IMBHs have remained elusive despite extensive searches.

However, in recent years there has been a surge in evidence supporting their existence. The detection of GW190521, a gravitational wave (GW) signal potentially arising from the merger of two SBHs, hints at the formation of an IMBH with a mass of approximately 142 $M_\odot$ (Abbott et al. 2020). Prior to this, the most compelling evidence for IMBHs stemmed from observations of active galactic nuclei (AGNs), such as the one in the galaxy NGC4395, hosting a BH with a mass of 3×10^5 $M_\odot$ solar masses (Peterson et al. 2005).One of the candidate globular clusters (GCs) to host an IMBH is ω-Cen, which has evidence for a stellar disc, suggesting the past existence of an inner gaseous disc (van de Ven et al. 2006; Mastrobuono-Battisti & Perets 2013).

Several formation channels have been proposed for IMBHs, including a direct collapse of gas at high redshifts (e.g. Eardley & Press 1975; Begelman, Volonteri & Rees 2006); remnants of the early population III ultra-massive stars in the Universe (e.g. Madau & Rees 2001); or runaway collisions and mergers of massive stars or BHs with main-sequence stars (e.g. Ebisuzaki et al. 2001; Portegies Zwart & McMillan 2002; Rose et al. 2022; Fujii et al. 2024).

IMBHs are expected to play a crucial role in various astrophysical phenomena: They may serve as seeds for the growth of SMBHs at the centres of galaxies (e.g. Madau & Rees 2001; Silk 2017); mergers of IMBHs with other compact objects could generate detectable GWs (e.g. Amaro-Seoane et al. 2007; Mandel et al. 2008; Gualandris & Merritt 2009; Fragione & Leigh 2018; Fragione et al. 2018); and tidal disruption events (TDEs) may occur when stars venture too close to IMBHs (e.g. MacLeod, Trenti & Ramirez-Ruiz 2016; Fragione et al. 2018).

The growing evidence for IMBHs, together with their potential astrophysical significance, has spurred renewed interest in their formation, evolution, and observational signatures.

It has been hypothesized that IMBHs could form and reside within GCs. Due to the processes of mass segregation and dynamical friction, these IMBHs are anticipated to migrate towards the central regions of GCs. Within these dense environments, they

★ E-mail: morozner@ias.edu

are likely to form binaries with stars or SBHs (Sigurdsson & Hernquist 1993). These binaries, through a process of hardening, could eventually become sources of GWs with distinctive mass ratios, namely extreme-mass ratio inspirals (EMRIs) with $10^{-8} \lesssim q = m_2/m_1 \lesssim 10^{-5}$, and intermediate-mass ratio inspirals (IMRIs) with $10^{-5} \lesssim q \lesssim 10^{-2}$ (Amaro-Seoane et al. 2007). Future space-based GW detectors such as *LISA* (Laser Interferometer Space Antenna) may be able to observe these unique signals (Amaro-Seoane et al. 2007; Amaro Seoane 2022).

Historically, GCs were believed to host a simple stellar population arising from a single burst of star formation. However, it is now understood that the majority of GCs contain at least two distinct populations (e.g. Bastian & Lardo 2015). While the origin of these multiple populations remains unclear, any episode of star formation necessitates the presence of a substantial amount of gas. Consequently, the first population stars and compact objects formed in GCs would later be embedded in a gas-rich environment that fostered the subsequent formation of second population stars. This gaseous environment could significantly influence the dynamical evolution of stars within the cluster.

Recent research has demonstrated that such gas-rich environments can serve as fertile grounds for various astrophysical phenomena, including gas-induced binary formation (Rowan et al. 2023; Rozner, Generozov & Perets 2023; Dodici & Tremaine 2024 Whitehead et al 2024a,b) and the generation of GWs (Rozner & Perets 2022). Other potential effects encompass the accretion-driven growth of stars and compact objects, gas-induced hierarchical mergers, spin alignment, and enhanced mass segregation and/or contraction of the cluster (see Leigh et al. 2013, 2014; Perets 2022, and references therein). Recently, many studies dealt with various aspects of the uniqueness of binary evolution in gas-rich environments (e.g. Li & Lai 2022, 2023a,b; Mishra & Calcino 2024; O'Neill et al. 2024; Rowan et al. 2024; Whitehead et al. 2024b and references therein), and still our physical understanding of these systems is far from being complete.

In this work, we study the evolution of IMBHs in gas-rich GCs. In this gas-rich environment, the IMBH would become embedded in gas, leading to the formation of a circumstellar disc analogous to those observed around SMBHs in AGNs, as illustrated on Fig. 3. We refer to such a system as a mini-AGN (mAGN). Notably, the formation of an mAGN does not require second-generation star formation necessarily; an accretion of gas from the interstellar medium or other external sources on to the cluster could also trigger this phenomenon (Lin & Murray 2007; Naiman, Ramirez-Ruiz & Lin 2011).

We study the conditions necessary for the formation of an mAGN disc and investigate its potential observational and theoretical implications for the dynamical evolution of stars within the cluster. The physics governing stars and compact objects embedded in AGN discs is complex and has been the subject of extensive research, particularly in recent years (e.g. Ostriker 1983; Artymowicz, Lin & Wampler 1993; McKernan et al. 2012; Stone, Metzger & Haiman 2017; Tagawa, Haiman & Kocsis 2020; Cantiello, Jermyn & Lin 2021; Li et al. 2023; Dodici & Tremaine 2024; Whitehead et al. 2024a). These studies have revealed a rich tapestry of dynamical processes, including gas-induced mergers of stars and SBHs, migration within the disc, the capture of stars and compact objects into the disc, accretion-driven growth, and the production of unique explosive transients and GW sources (e.g. Artymowicz et al. 1993; McKernan et al. 2012; Bartos et al. 2017; Stone et al. 2017; Tagawa et al. 2020; Grishin et al. 2021; Samsing et al. 2022; Vaccaro et al. 2024). It is reasonable to expect that many of these processes (and some others), albeit with modifications, could also transpire within the context of mAGNs.

In Section 2, we characterize the available parameter space for the mAGNs. In Section 3, we discuss different models for motion in gas. In Section 3.1, we discuss disc migration. In Section 3.2, we briefly introduce gas dynamical friction (GDF). In Section 4, we discuss some of the possible dynamical processes expected in mAGNs, including alignment into an mAGN (Section 4.2), GW mergers (Section 4.3), and TDEs (Section 4.4). In Section 5, we discuss the formation of accreting IMBHs from capture binaries. In Section 6, we discuss the formation of large-scale jets. We then discuss our results and possible implications in Section 7, introduce possible caveats in Section 8, and finally conclude and summarize in Section 9.

2 PARAMETER SPACE OF THE DISC

Let us consider a GC during the formation of its second (or further) generation of stars, which also harbours an IMBH. During this phase, a pre-existing IMBH within the GC would be embedded in gas, leading to the formation of an accretion disc around the IMBH. We aim to constrain the parameters of this disc using analytical arguments and a numerical solution of the accretion disc equations as presented in Sirko & Goodman (2003) and Gangardt et al. (2024).

A mass inflow into the disc persists as long as gas is present within the cluster. However, the gas is expelled from the cluster upon the emergence of the first supernovae, establishing a maximum typical gas lifetime of roughly $\sim$10–10^2 Myr (Bastian & Lardo 2015). It should be noted that this assumption is somewhat conservative. The continuous mass-loss from giant stars provides a sustained gas supply, a portion of which is expected to accrete on to the IMBH even at later times. Furthermore, as previously mentioned, additional potential sources of gas accretion on to the cluster could replenish the gas supply to the IMBH.

Afterwards, the gas depletes within a typical viscous time, given by

$$\tau_v = \frac{1}{\alpha\Omega}\left(\frac{h}{r}\right)^{-2} = \left(\frac{0.01}{\alpha}\right)\left(\frac{6.47\times10^{-10}\ \mathrm{s}^{-1}}{\Omega}\right)\left(\frac{h/r}{0.01}\right)^{-2} \approx 49\ \mathrm{Myr}, \quad (1)$$

where α is the Shakura–Sunyaev parameter (Shakura & Sunyaev 1973), Ω is the Keplerian angular frequency, and h/r is the aspect ratio of the disc.

We calculate the Safronov–Toomre stability parameter (Safronov 1960; Toomre 1964) for different disc radii and IMBH masses. The gravitational stability of the disc could be determined by

$$Q = \frac{c_{\mathrm{s,mAGN}}\Omega}{\pi G\Sigma} = \frac{hM_{\mathrm{IMBH}}}{\sqrt{2}\pi\Sigma R^2} = \frac{M_{\mathrm{IMBH}}}{\sqrt{8}\pi\rho_{\mathrm{mAGN}}R^3}, \quad (2)$$

where $c_{\mathrm{s,mAGN}}$ is the sound speed in the mAGN, Σ is the surface density, h is the scale height of the mAGN disc, M_{IMBH} is the mass of the IMBH, ρ_{mAGN} is the mid-plane density, and R is the distance from the centre. Note that we relate here everywhere to the mid-plane gas density. In Fig. 1, we present the value of Q for different combinations in the parameter space. The yellow area marks the available parameters for a stable disc according to this criterion, i.e. $Q \geq 1$. The Safronov–Toomre parameter shown here is local in the sense that we compare the local contribution from gravity to the one from thermal pressure.

In Fig. 1, we present the Safronov–Toomre parameter for different choices of M_{IMBH}, radii, and gas densities, as calculated using equation 2. We set the available parameter space for stable mAGN discs and specifically the largest radius allowed for a stable disc,

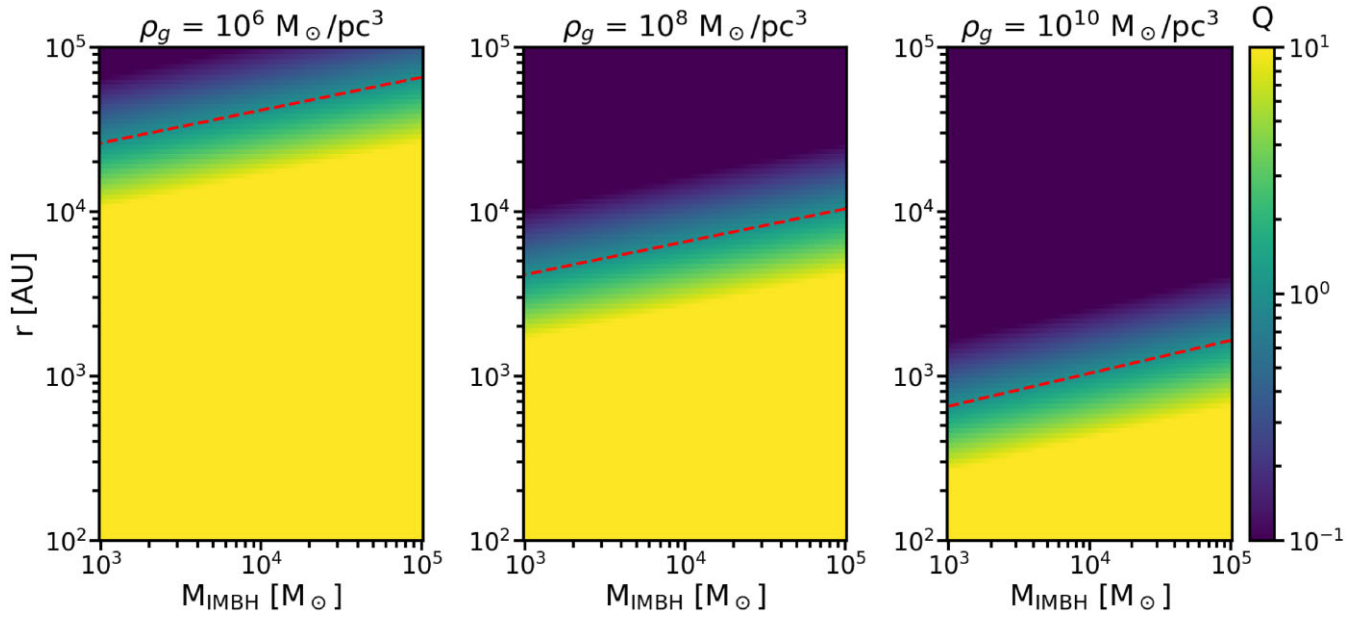

Figure 1. The Safronov–Toomre parameter (equation 2) as calculated for different possible disc parameters, assuming a temperature of $T = 10^5$ K. The dashed lines indicate the maximal allowed radius ($Q = 1$), such that all of the radii below the dashed line will have a stable disc ($Q > 1$), and all the radii above the dashed line will have an unstable disc ($Q < 1$). Different panels stand for different densities, assuming a constant density through the disc.

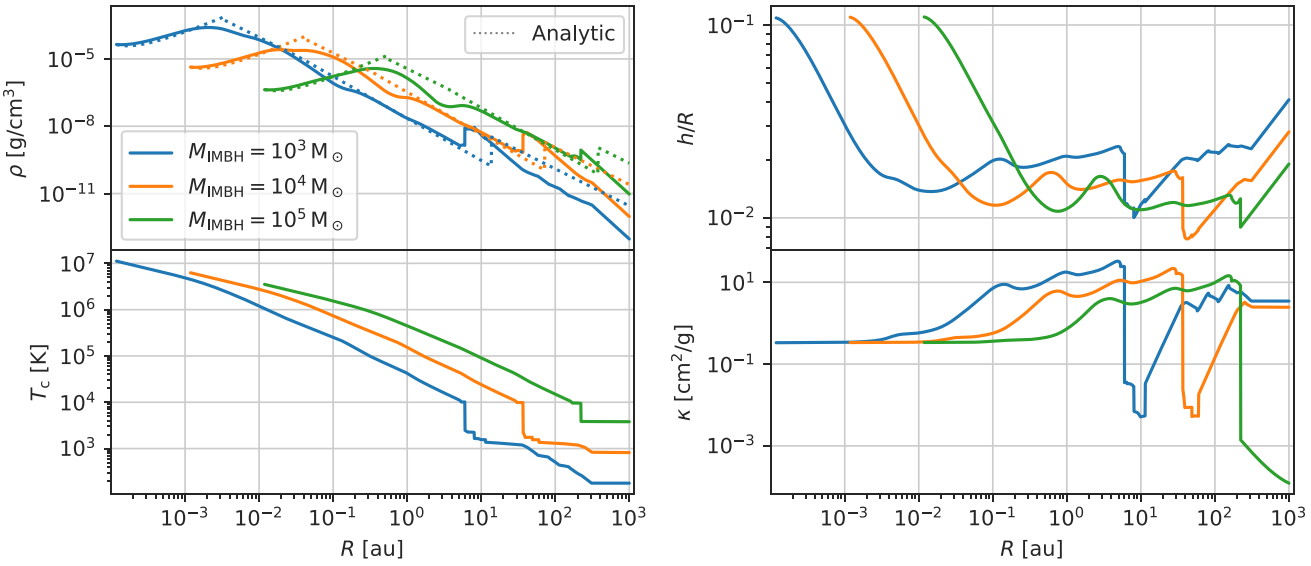

Figure 2. Various profiles of the three Sirko & Goodman (2003) discs around an IMBH considered here. Top-left panel: Gas density. Top-right panel: Aspect ratio of the disc. Bottom-left panel: Mid-plane temperature. Bottom-right panel: Opacity corresponding to IMBH masses of $M_{\rm IMBH} = 10^3$, 10^4, and 10^5 M$_\odot$.

given a mass of a central IMBH. The typical radius of an mAGN disc of gas density 10^{10} M$_\odot$ pc^{-3} surrounding a 10^4 M$_\odot$ IMBH will be $\sim 10^3$ au.

In Fig. 2, we present the numerical solution for an mAGN using the Sirko & Goodman (2003) equations. We modelled three α-discs (i.e. with the viscosity being proportional to the total pressure; see Haiman, Kocsis & Menou 2009), for IMBH masses $M_{\rm IMBH} = 10^3$, 10^4, and 10^5 M$_\odot$, assuming a viscosity parameter of $\alpha = 0.1$ and a mass accretion $\dot{M} = 0.5\dot{M}_{\rm Edd}$, where

$$\dot{M}_{\rm Edd} = \frac{L_{\rm Edd}}{\epsilon c^2} \tag{3}$$

is the Eddington accretion rate, $L_{\rm Edd}$ is the Eddington luminosity, and $\epsilon = 0.1$ is the radiation efficiency (for more details, see Gangardt et al. 2024).

The models with $M_{\rm IMBH} = 10^3$ and 10^4 M$_\odot$ exhibit the so-called opacity gap, the drop in opacity at temperatures of $T \approx 10^3$–10^4 K, at a radius of 10–70 au, while the $M_{\rm IMBH} = 10^5$ M$_\odot$ disc, being more massive and hotter, enters the opacity gap only in the outermost region ($\sim$200 au).

The gas density in the disc is higher than in AGN discs, as the gas is concentrated in a smaller region, as expected also from the crude estimate (see also Cantiello et al.

2021)

$$\rho_{\rm g} \sim \frac{M_{\rm IMBH}}{\sqrt{8}\pi\, R^3} \sim 10^{10} \frac{\rm M_\odot}{\rm pc^3} \frac{M_{\rm IMBH}}{10^4\ \rm M_\odot} \left(\frac{10^3\ \rm au}{R_{\rm disc}}\right)^3. \quad (4)$$

This will lead in turn to enhanced rates of migration in the disc, as discussed below.

The models introduced in Sirko & Goodman (2003) do not prescribe an outer boundary of the disc. Such outer boundary is dictated by other constraints. In Sirko & Goodman (2003), the consistency of the modelled spectral energy distribution with the observations determines the outer boundary. Given that no current mAGN has yet been identified, because they exist for short time-scales, exist only during early times of GCs' formation, or their properties are beyond the current observational capabilities, we cannot rely on observations, in this regard, and instead truncate the disc at 10^3 au, which is a fraction of the average interparticle distance in the core of a GC ($\sim 1.3 \times 10^4$ au for a core number density of 5×10^3 pc^{-3}). The mass of objects embedded in the disc could not exceed the mass of the disc, on the very extreme side, to maintain stability, which sets an upper bound on the number of objects in the disc. A more conservative and realistic assumption would be no more than $\sim$10 per cent of the disc mass. The mass of the disc up to the 10^3 au is approximately 100, 800, and 4600 $\rm M_\odot$ for $M_{\rm IMBH} = 10^3$, 10^4, and $10^5\ \rm M_\odot$, respectively. Hence, the disc cannot host more than $\sim$10, 80, and 460 solar-mass stars correspondingly or $\sim$1, 8, and 46 BHs with mass 10 $\rm M_\odot$.

3 MOTION IN GAS

The dynamics of objects embedded in gas-rich environments deviate significantly from their evolution in a vacuum. Several approaches can be employed to model this behaviour, including mini-discs (Stone et al. 2017), migration within discs (McKernan et al. 2012), and modelling based on Bondi–Hoyle–Lyttleton supersonic flows and their associated energy dissipation (Antoni, MacLeod & Ramirez-Ruiz 2019).

The evolution within AGN discs is a complex and not fully understood phenomenon, with even the direction of migration torques remaining a subject of debate (Moody, Shi & Stone 2019; Duffell et al. 2020; Muñoz et al. 2020; Grishin, Gilbaum & Stone 2024). In this study, we will apply the conditions of an mAGN disc to investigate the evolution of objects within the disc under the influence of both type I/II migration and GDF, comparing the results obtained from these two distinct approaches. Additionally, we will employ various density models, including a broken power-law model (Grishin et al. 2024) based on the numerical solution of Gangardt et al. (2024), as well as flat density profiles with varying densities.

3.1 Gas-induced migration in gaseous discs

The migration of objects embedded within an accretion disc can also be modelled by utilizing the migration torques originally derived in the context of planet formation and evolution. In this framework, migration is typically categorized into two regimes: type I and type II. Type I migration is relevant for low-mass planets, where their interaction with the disc is relatively weak. In this regime, the torque driving migration arises from the gravitational interaction between the planet and the density waves it excites within the disc (Ward 1997; Tanaka, Takeuchi & Ward 2002; Paardekooper et al. 2010).

The torque is given by

$$\Gamma_{\rm I} \approx -\left(\frac{m}{M_{\rm cen}}\right)^2 \left(\frac{h}{r}\right)^{-2} \Sigma_{\rm g} r^4 \Omega_{\rm K}^2, \quad (5)$$

where m is the mass of the migrating object, $M_{\rm cen}$ is the mass of the central object, $\Sigma_{\rm g}$ is the surface density of the disc, r is the radial distance from the central object, $\Omega_{\rm K}$ is the Keplerian angular velocity, and h/r is the aspect ratio of the disc. Note that there might be some order of unity corrections due to the disc structure, which we will neglect.

More massive planets could potentially open a gap in the disc and, for them, the torque is dominated by the viscous evolution of the disc as it interacts with the gap (Lin & Papaloizou 1979a,b, 1986; Ward 1997; Ida & Lin 2004; Duffell et al. 2014; Kanagawa, Tanaka & Szuszkiewicz 2018). In this regime, the torque is given by

$$\Gamma_{\rm II} \approx -3\pi\alpha \left(\frac{h}{r}\right)^2 \Sigma_{\rm g} r^4 \Omega_{\rm K}^2, \quad (6)$$

where α is the Shakura–Sunyaev parameter of the disc (Shakura & Sunyaev 1973).

The total torque exerted on a migrating planet depends on the regime, such that

$$\Gamma_{\rm tot} = \begin{cases} \Gamma_{\rm I}, & R_{\rm Hill} < H, \\ \Gamma_{\rm II}, & R_{\rm Hill} > H, \end{cases} \quad (7)$$

where $R_{\rm Hill} = r\,(M_\star/3M_{\rm IMBH})^{1/3}$ is the Hill radius and the migration rate is given by

$$\frac{{\rm d}r}{{\rm d}t} = \frac{2\Gamma_{\rm tot}}{mr\Omega_{\rm K}}. \quad (8)$$

3.2 Gas dynamical friction

Here, we use the GDF model (Ostriker 1999). The interaction of an object with a non-zero velocity relative to the background gas dissipates energy from the binary and hence leads to hardening. The GDF force is given by

$$\boldsymbol{F}_{\rm GDF} = -\frac{4\pi G^2 m^2 \rho_{\rm g}}{v_{\rm rel}^3} \boldsymbol{v}_{\rm rel} I\left(\frac{v_{\rm rel}}{c_{\rm s}}\right), \quad (9)$$

where m is the mass of the object, $\rho_{\rm g}$ is the gas density, $v_{\rm rel}$ is the relative velocity between the gas and the object, and I is a function of $v_{\rm rel}$ and the speed of sound $c_{\rm s}$, given by

$$I(\mathcal{M}) = \begin{cases} \frac{1}{2}\ln\frac{1+\mathcal{M}}{1-\mathcal{M}} - \mathcal{M}, & \mathcal{M} < 1, \\ \frac{1}{2}\ln\frac{\mathcal{M}+1}{\mathcal{M}-1} + \ln\frac{\mathcal{M}-1}{r_{\rm min}/c_{\rm s}t}, & \mathcal{M} > 1. \end{cases} \quad (10)$$

The separation evolution for a circular orbit is then given by (Murray & Dermott 2000; Grishin & Perets 2016)

$$\left.\frac{{\rm d}a}{{\rm d}t}\right|_{\rm GDF} = \frac{2a^{3/2}}{\sqrt{G(m_1+m_2)}} \Delta f_{{\rm GDF},\theta}, \quad (11)$$

where $\Delta \boldsymbol{f}_{\rm GDF}$ is the differential force per mass between the binary components, and $f_{{\rm GDF},\theta}$ is its tangential component.

$$\Delta \boldsymbol{f}_{\rm GDF} \propto m_1 \frac{\boldsymbol{v}_{{\rm rel},1}}{v_{{\rm rel},1}^3} - m_2 \frac{\boldsymbol{v}_{\boldsymbol{\rm rel},2}}{\boldsymbol{v}_{\boldsymbol{\rm rel},2}^3},$$
$$\boldsymbol{v}_{{\rm rel},1} = \boldsymbol{V}_{\rm cm} + \frac{m_2}{m_1+m_2}\boldsymbol{v},\ \boldsymbol{v}_{\boldsymbol{\rm rel},2} = \boldsymbol{V}_{\rm cm} - \frac{m_1}{m_1+m_2}\boldsymbol{v}, \quad (12)$$

where $\boldsymbol{V}_{\rm cm}$ is the centre-of-mass velocity and $\boldsymbol{v}$ is the relative velocity between the binary components m_1 and m_2. We consider the centre-of-mass velocity $V_{\rm cm}$ to be the velocity dispersion of the binary and

Table 1. The fiducial values used in the paper unless stated otherwise.

Notation	Name	Fiducial value
$M_{\rm IMBH}$	IMBH mass	10^4 M$_\odot$
$R_{\rm mAGN}$	Radius of the mAGN	1–2 $\times$ 10^3 au
$M_{\rm mAGN}$	mAGN mass	1200 M$_\odot$
h/r	Aspect ratio	0.01–0.05
α	Viscosity parameter	0.01
$\tau_{\rm gas}$	Gas lifetime	50 Myr

$v = v_{\rm Kep}$. In the supersonic regime, in which we focus, $\sigma \ll v_{\rm Kep}$ and hence one can neglect the contribution from $V_{\rm cm}$. Under these assumptions, the differential equation for the separation evolution could be reduced to

$$\left.\frac{{\rm d}a}{{\rm d}t}\right|_{\rm GDF} = -\frac{8\pi G^{3/2}a^{3/2}}{\sqrt{m_1+m_2}}\rho_{\rm g}(t)\frac{m_1}{v_{\rm Kep}^2} I\left(\frac{v_{\rm Kep}}{c_{\rm s}}\right)\xi(q), \quad (13)$$
$$\xi(q) = \left[(1+q^{-1})^2 + q(1+q)^2\right],$$

where $q = m_2/m_1$ is the mass ratio of the binary. Note that this equation differs from equation 7 in Rozner et al. (2023) by a factor of unity, due to mass-ratio corrections.

This equation could be solved analytically, assuming that I could be approximated by a constant for the motion, leading to the solution

$$a(t) \approx \left(\frac{3}{2}\left[A\tau_{\rm gas}e^{-t/\tau_{\rm gas}} + C\right]\right)^{-2/3},$$
$$A = \frac{8\pi G^{1/2}}{(m_1+m_2)^{3/2}}\rho_{\rm g,0}m_1 I\xi(q),$$
$$C = \frac{2}{3}a_0^{-3/2} - A\tau_{\rm gas}. \quad (14)$$

For very long time-scales ($t/\tau_{\rm gas} \gg 1$), the solution converges towards an asymptote,

$$a(t\to\infty) = \left(\frac{3}{2}C\right)^{-2/3}. \quad (15)$$

Moreover, it can be seen that the $\dot{a}|_{\rm GDF} \propto a^{2.5}$, such that once small enough separations are reached, GDF will become inefficient.

The typical time-scale for a significant change due to GDF is given by

$$\tau_{\rm GDF} = \left|\frac{a}{\dot{a}|_{\rm GDF}}\right| \approx (Aa^{3/2})^{-1}, \quad (16)$$

where we assumed that this time-scale is much shorter than the gas lifetime (which is justified later by the full solutions).

4 DYNAMICAL PROCESSES

Here, we will sketch the dynamical processes induced by the presence of mAGN in a GC. We specify our fiducial parameters, in Table 1, which are used throughout, unless stated otherwise.

4.1 Gas hardening

Both disc migration and GDF extract energy from the binary, leading to a separation decrease, i.e. gas hardening of the binary.

Fig. 4 illustrates the migration of objects within an mAGN disc under the influence of disc migration. The upper left panel depicts the time evolution of the separation between the IMBH and objects of varying masses. It is evident that the evolutionary tracks diverge significantly for different masses, with more massive objects exhibiting faster migration rates. Furthermore, after a while, the separation reaches an equilibrium value that is mass-dependent. The upper right panel showcases the time evolution of the density profile, assuming an exponential decay with a characteristic time-scale of 50 Myr. The lower left panel presents the separation evolution for various initial separations, revealing a weak dependence on the initial conditions. The lower right panel demonstrates the evolution of a solar-mass star within mAGN discs surrounding IMBHs of different masses. Notably, higher IMBH masses result in faster migration rates and distinct final separations. Across all the evolutionary plots, multiple evolution regimes are observed, governed by migration into different density regions of the disc (refer to the upper right panel for the density profile). The rapid migration of objects with diverse masses towards a common small separation could potentially catalyse collisions and trigger the formation of transient phenomena.

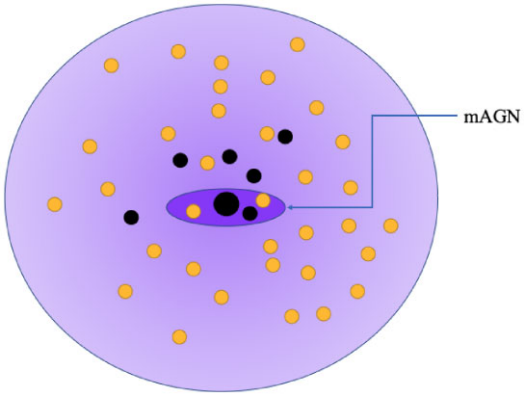

Figure 3. An illustration not to scale of the gas-rich cluster (in purple), the mAGN embedded in it (in dark purple), stars (in yellow), and BHs (in black).

Fig. 5 illustrates the evolution of objects within the mAGN disc solely under the influence of GDF. The upper left panel displays the time evolution of separation for objects of varying masses. It is apparent that GDF is a highly efficient mechanism, causing a substantial separation shrinkage over remarkably short time-scales, potentially even less than a year. Interestingly, more massive objects exhibit slower migration, although this migration saturates after a brief period as the separation becomes very small. This diminished separation results in a high relative velocity between the object and the gas, rendering GDF less effective (since $F_{\rm GDF} \propto v_{\rm rel}^{-3}$).

The upper right panel underscores the crucial role of GDF in GW emission. In the absence of gas, no GW emission is anticipated under these conditions. However, the introduction of gas leads to an expected merger within a relatively short time frame. The lower left panel presents the evolutionary tracks for objects starting from different initial separations. Due to the high efficiency of GDF, the dependence on the initial separation is weak, with all curves converging after a short duration. The lower right panel showcases the evolution of a star within discs surrounding IMBHs of varying masses. It is observed that higher IMBH masses correspond to more efficient migration.

4.2 Alignment into the disc

Consider a star with mass $m_\star$ in an inclined orbit with respect to the disc. The typical time-scale to dissipate the velocity with GDF could be estimated by (e.g. Artymowicz et al. 1993; Rein 2012; Bartos et al. 2017; Panamarev et al. 2018; Fabj et al. 2020; Generozov &

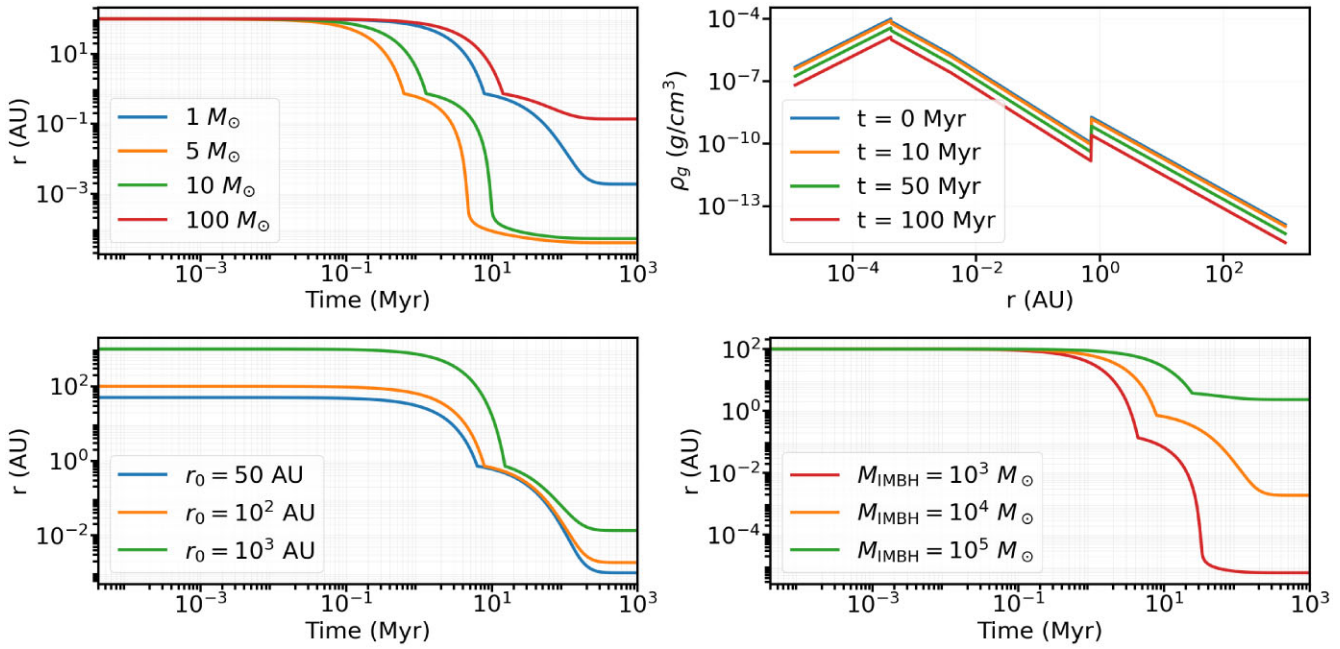

Figure 4. The evolution of objects under the effect of *disc migration* only, in an mAGN disc with a radius of 1000 au, $\alpha = 0.01$, $h/r = 0.05$, and typical gas lifetime of 50 Myr with an exponential decay. Unless stated otherwise, the default parameters that we vary are $M_{\rm IMBH}$, gas density profile as described in Fig. 2, initial separation of 10^2 au, and solar-mass migrating star. Upper left: Evolution in time of the separation between the IMBHs and objects of different masses. Upper right: Evolution in time of the gas density profile described in Fig. 2 for an IMBH of mass 10^4 M$_\odot$. Lower left: Evolution in time of the separation, for different given separations (note the different y-axis). Lower right: Migration for different masses of the IMBH.

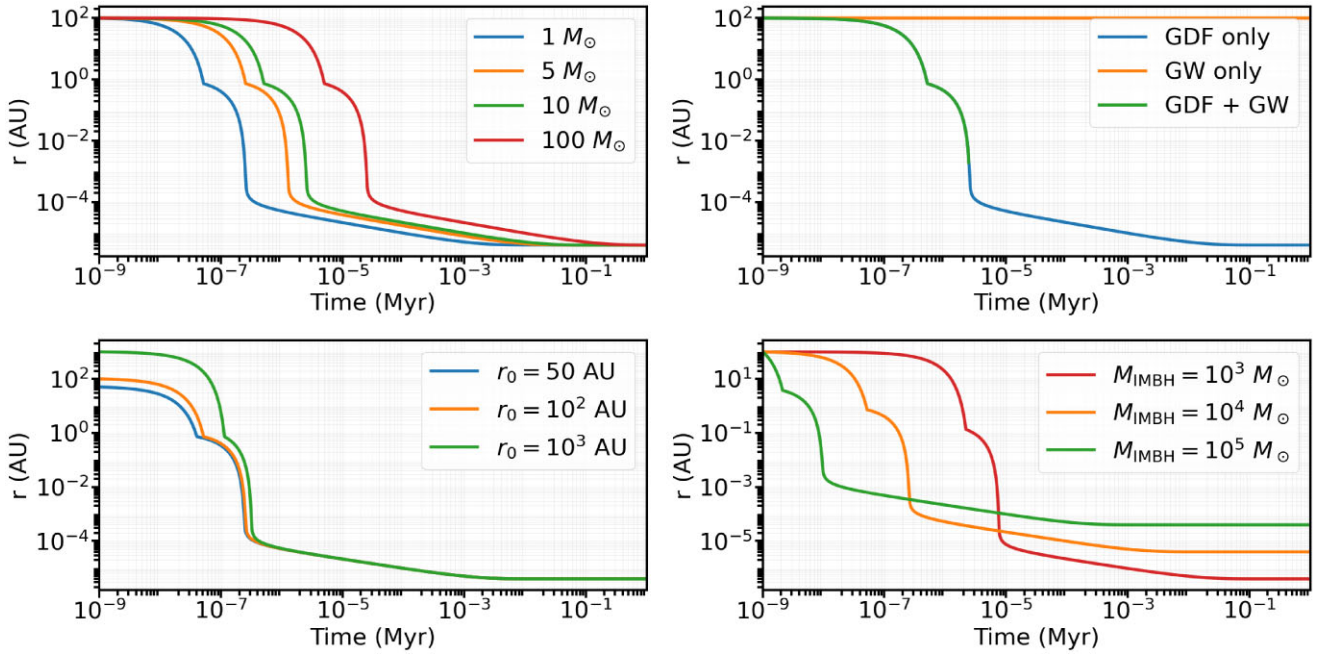

Figure 5. The evolution of objects under the effect of GDF only, in an mAGN disc with a radius of 1000 au, $\alpha = 0.01$, $h/r = 0.05$, and typical gas lifetime of 50 Myr with an exponential decay. Unless stated otherwise, the default parameters that we vary are $M_{\rm IMBH}$, gas density profile as described in Fig. 2, initial separation of 10^2 au, and solar-mass migrating star. Upper left: Evolution in time of the separation between the IMBHs and objects of different masses. Upper right: Comparison between the evolution under GDF only, GW only, and the combined effect of the two, for a 10 M$_\odot$ object migrating in a disc surrounding a 10^4 M$_\odot$ IMBH. Lower left: Evolution in time of the separation, for different given separations. Lower right: Migration for different masses of the IMBH.

Perets 2023; Nasim et al. 2023)

$$\tau_{\rm align} \sim \frac{v_{\rm Kep}^3(a)}{G^2 \rho_{\rm g} m \frac{h}{r} \ln \Lambda} \sin^3 \frac{i}{2} \sin i. \quad (17)$$

Fig. 6 presents the alignment time-scales for solar-mass objects as a function of gas density and semimajor axis. For typical gas densities, the alignment time-scales with the disc are short, often shorter than the gas lifetime itself. This suggests that all or the vast

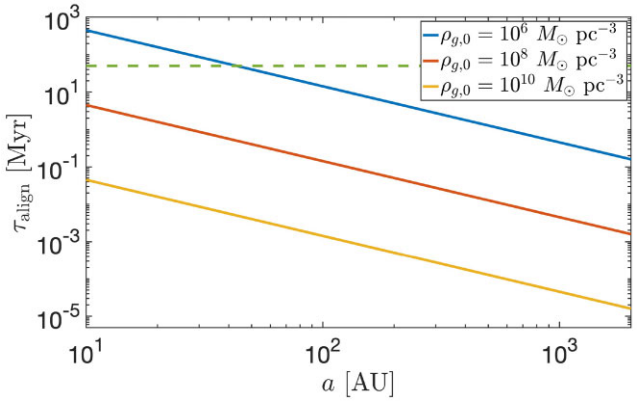

Figure 6. Typical alignment time-scales for a solar-mass star with an inclination of $\pi/2$, for different gas densities (solid lines), in comparison to the gas lifetime (dashed line). These densities correspond to 7×10^{-17}, 7×10^{-15}, and 7×10^{13} g cm^{-3} correspondingly.

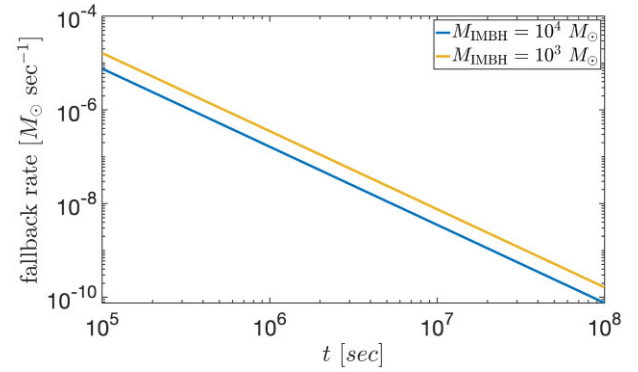

Figure 7. Approximate late times rate for a solar-mass star and an IMBH with masses of $10^3/10^4$ M$_\odot$.

majority of solar-mass objects are expected to align with the disc plane.

However, the number of objects that can align with the disc is limited by stability considerations related to the disc's mass, as discussed earlier. In general, larger discs capable of hosting a sufficient number of stars may allow massive perturbers to align via resonant dynamical friction (Ginat et al. 2023).

4.3 Gravitational wave mergers

Gas hardening, the process by which the energy of binaries dissipates more rapidly in the presence of gas, can act as a catalyst for GW mergers. This phenomenon has been demonstrated in the context of gas-rich GCs (Rozner & Perets 2022) and other gaseous environments such as AGN discs (McKernan et al. 2012; Stone et al. 2017; Tagawa et al. 2020).

Mini-AGNs, by their nature, could harbour binaries comprising the IMBH and a companion object. These binaries have the potential to become sources of IMRIs or, in the case of massive IMBHs, EMRIs. Traditionally, EMRIs are thought to arise from two-body encounters (two-body relaxation) at the centres of dense stellar nuclei, tidal-induced binary separation, or migration (Hopman & Alexander 2005; Miller et al. 2005; Levin 2007; Amaro-Seoane 2018; Raveh & Perets 2021). However, within gas-rich media, alternative formation channels become viable.

There are several unique features to the GWs' channel described above. The effect of gas hardening could shift the frequency of the produced GWs (see a discussion on frequency shifting in a different context in Tanaka 2008; Hendriks, Zwick & Samsing 2024; Samsing et al. 2024):

$$\frac{\Delta f}{f} \approx \frac{T_{\mathrm{obs}}}{\tau_{\mathrm{merge}}}, \tag{18}$$

where f is the observational frequency band, T_{obs} is the duration of the observation, which is typically 1 yr, and $\tau_{\mathrm{merge}} \approx 20$ yr is the typical merger time-scale for $\rho_{\mathrm{g},0} = 10^{10}$ M$_\odot$ pc^{-3}.

The frequency shift translates to a shift in the number of cycles before the plunge,

$$\Delta N \approx \Delta f T_{\mathrm{obs}} = f T_{\mathrm{obs}} \frac{T_{\mathrm{obs}}}{\tau_{\mathrm{merge}}} \approx 1577, \tag{19}$$

for $f = 10^{-3}$ Hrz, which is the observational frequency of *LISA*. Since the typical number of cycles is $N \sim f T_{\mathrm{obs}} \sim 31\,557$, the number of extra orbits is significant (∼5 per cent increment). For smaller gas densities, such as $\rho_{\mathrm{g},0} = 10^6$ M$_\odot$ pc^{-3}, $\tau_{\mathrm{merge}} \approx 2 \times 10^{-2}$ Myr, which translates to a shift of $\Delta N \approx 1.6$, which in principle could be observed as well. A larger number of cycles could improve our observational understanding of the shape of these GWs.

IMBH–BH mergers could potentially be highly misaligned unless there is a spin-up induced by accretion that leads to alignment. Misaligned mergers could lead to high-velocity GW kicks. Strong enough kicks could eventually deplete the GC from IMBHs.

The existence of mAGN discs could also increase the production rates of GW sources, and specifically the rates of IMRIs, and hereby we will estimate the BH–IMBH merger rate, considering a BH with mass 10 M$_\odot$ and an IMBH with mass 10^4 M$_\odot$. This rate is sensitive to the assumptions on several distributions, as we will describe below. The rate is then given by

$$\Gamma \sim f_{\mathrm{IMBH}}^{\mathrm{GC}} \frac{n_{\mathrm{GC}} N_\star f_{\mathrm{mAGN}} f_{\gtrsim 20\ \mathrm{M}_\odot} f_{\mathrm{ret}} f_{\mathrm{merge}}}{\tau_{\mathrm{GC}}}, \tag{20}$$

where $f_{\mathrm{IMBH}}^{\mathrm{GC}}$ is the fraction of GCs that host an IMBH, n_{GC} is the number density of GCs, $N_\star$ is the number of stars in the cluster, f_{mAGN} is the fraction of stars from the cluster that reside in the mAGN disc, $f_{\gtrsim 20\ \mathrm{M}_\odot}$ is the fraction of stars with masses larger than 20 M$_\odot$, f_{ret} is the retention fraction in the cluster, and f_{merge} is the fraction of binaries that merge. We take the lifetime of the GC as 10 Gyr.

The fraction of GCs harbouring an IMBH is highly uncertain, contingent upon various factors including IMBH formation and retention within the cluster. Following Fragione (2022) and Tang et al. (2024), we adopt an occupation fraction ($f_{\mathrm{IMBH}}^{\mathrm{GC}}$) ranging between 0.01 and 0.1. The number density of GCs is taken to be within the range of (0.33–3) $\times 10^9$ Gpc^{-3}, in accordance with Kritos & Cholis (2020).

Stability considerations dictate that the total number of BHs within the mAGN cannot surpass 10, implying $N_\star f_{\mathrm{mAGN}} f_{\gtrsim 20\ \mathrm{M}_\odot} f_{\mathrm{ret}} \leq 10$. For the lower bound, we factor in the alignment of binaries into the disc from the surrounding sphere. As illustrated in Fig. 6, the alignment time-scales are sufficiently short to consider the entire sphere around the mAGN disc, as objects will eventually align within the disc's lifetime. This translates to $f_{\mathrm{mAGN}} \sim (R_{\mathrm{mAGN}}/R_{\mathrm{GC}})^3 \sim 10^{-7}$ for $R_{\mathrm{mAGN}} \sim 10^3$ au and $R_{\mathrm{GC}} \sim$ pc.

We employ a Kroupa mass function (Kroupa 2002) for the cluster, resulting in a fraction of stars with masses exceeding 20 M$_\odot$ of 2×10^{-3} in a non-segregated environment. The retention fraction within the cluster is assumed to be 10 per cent (Kritos & Cholis 2020). Based on our model, we set the merger fraction (f_{merge})

to 1. Under these assumptions, the merger rate resulting from our proposed channel ranges between $\sim 7 \times 10^{-10}$ and 0.03 $\mathrm{Gpc^{-3}\ yr^{-1}}$. It should be noted that even under optimistic assumptions, one can restrict the number of mergers to not exceed one merger during the lifetime of the mAGN, due to GW kicks that can destroy the disc. Hopefully, with future measurements, some of the uncertainties will be cleared, leading to a more constraining rate calculation. This range can potentially contribute to the typically expected observational rates of 0.1–10 $\mathrm{Gpc^{-3}\ yr^{-1}}$ (Abbott et al. 2017, 2019, 2022; Fragione 2022).

4.4 Tidal disruption events

The dynamics in the mAGN could lead to the disruption of stars by the IMBH, producing a unique type of TDEs, with typical masses 10^{-3} to 10^{-2} smaller than the masses of the 'standard' TDEs produced by interactions with MBHs, and hence we term as milli-TDEs (mTDEs) and centi-TDEs (cTDEs) correspondingly. The tidal disruption radius is given by

$$R_{\rm t} = R_\star \left(\frac{M_{\rm IMBH}}{M_\star}\right)^{1/3}, \tag{21}$$

which is 22 $\mathrm{R_\odot}$ approximately for $R_\star = \mathrm{R_\odot}$, $M_\star = \mathrm{M_\odot}$, and $M_{\rm IMBH} = 10^4\ \mathrm{M_\odot}$. For an mTDE to occur, the disrupted object should pass by the IMBH at a distance that does not exceed the tidal disruption radius. Such a close encounter could take place by either a random close encounter or a gas-assisted encounter.

The most bound material first returns to the pericentre after a typical time-scale given by (e.g. Rees 1988; Perets et al. 2016)

$$t_{\rm min} = \frac{2\pi R_{\rm t}^3}{(GM_{\rm IMBH})^{1/2}(2R_\star)^{3/2}} \approx 3\times 10^5\ \mathrm{s} \left(\frac{R_\star}{\mathrm{R_\odot}}\right)^{3/2} \left(\frac{M_{\rm IMBH}}{10^4\ \mathrm{M_\odot}}\right)^{1/2} \left(\frac{\mathrm{M_\odot}}{M_\star}\right).$$

The bound material then returns to the pericentre at a rate given by

$$\dot{M}(t) = \frac{1}{3}\frac{M_\star}{t_{\rm min}} \left(\frac{t}{t_{\rm min}}\right)^{-5/3}. \tag{22}$$

Generally, $\mathrm{d}M/\mathrm{d}E$, i.e. mass per unit energy, varies with the strength of the tidal interaction and the density profile of the disrupted objects. For completely disrupted objects, this dependence is relatively flat, such that for late times, $\dot{M} \propto t^{-5/3}$.

On Fig. 7, we present the fallback rate as a function of time, for different IMBH masses.

The event rate of cTDEs per cluster could be estimated by

$$\Gamma_{\rm cTDE} \approx N_{\rm IMBH} \frac{2\pi G(M_{\rm IMBH} + M_\star)N_\star R_{\rm t}}{\sigma V_{\rm c}} \approx 0.18\ \mathrm{Myr^{-1}}, \tag{23}$$

where $N_{\rm IMBH}$ is the number of IMBHs in the cluster, $N_\star$ is the number of stars, $R_{\rm t} = R_\star\,(M_{\rm IMBH}/M_\star)^{1/3}$ is the tidal radius, and $V_{\rm c} \approx 4\pi R_{\rm cl}^3/3$ is the volume of the cluster. Here, we assume that the cross-section is dominated by gravitational focusing and that in practice the TDE rate is determined by the collision rates of IMBHs. Here, we considered $M_{\rm IMBH} = 10^4\ \mathrm{M_\odot}$, $M_\star = \mathrm{M_\odot}$, $N_\star = 10^5$, $R_\star = \mathrm{R_\odot}$, $\sigma = 20\ \mathrm{km\,s^{-1}}$, and $\mathrm{R_{cl}} = \mathrm{pc}$.

The peak luminosity of a cTDE is expected to be the Eddington luminosity, and hence the typical peak luminosity of a cTDE is expected to be 10^{-3} to 10^{-2} weaker than the one of a standard TDE. It should be noted that while cTDE could be just limited by Eddington, in some cases, we might get a jet that might be far more luminous (see discussion in the context of μTDE in Perets et al. 2016).

5 FORMATION OF ACCRETING IMBHS FROM CAPTURED BINARIES

The presence of an IMBH embedded in a gas-rich environment, as envisioned in our proposed mAGN scenario, presents the opportunity for the formation of accreting systems akin to ultraluminous X-ray sources (ULXs). This process can be initiated when stars or binaries migrate through the disc and are subsequently captured by the IMBH, potentially resulting in mass transfer and accretion. Currently, several lines of evidence suggest the presence of IMBHs in ULXs [for a comprehensive review, refer to Kaaret, Feng & Roberts (2017) and references therein].

Below, we discuss the formation of accreting IMBHs from binary companions captured due to migrating stars in the AGN disc.

5.1 Formation of accreting systems

Once a binary system is captured by the IMBH, it can undergo evolution into an accreting system via multiple pathways:

(1) **Direct capture of a binary:** In the event of a tight binary being captured, the less massive component may expand to fill its Roche lobe, leading to mass transfer on to the IMBH and the establishment of an accreting system (Hopman, Portegies Zwart & Alexander 2004).

(2) **Tidal capture of a single star:** A single star can be tidally captured by the IMBH. Subsequently, the star may evolve to fill its Roche lobe, initiating mass transfer and accretion on to the IMBH (Hopman et al. 2004; Patruno et al. 2006).
The typical rate for such a tidal capture per an IMBH could be estimated by

$$\Gamma_{\rm tc} = n\pi R_{\rm t}^2 \left(1 + \frac{2GM_{\rm IMBH}}{R_{\rm t}\sigma_\star^2}\right)\sigma_\star \approx 10^{-5}\ \mathrm{Myr^{-1}}, \tag{24}$$

$$R_{\rm t} = R_\star \left(\frac{M_{\rm IMBH}}{m_\star}\right)^{1/3}, \tag{25}$$

when we considered the parameters of a star with a solar mass and a solar radius, $\sigma_\star = 10\ \mathrm{km\,s^{-1}}$, and $M_{\rm IMBH} = 10^4\ \mathrm{M_\odot}$. It should be noted that the cross-section can change due to the presence of gas.

(3) **Exchange interactions:** In a dense environment, the IMBH may acquire a stellar companion through exchange interactions with existing binaries (Mapelli, Zampieri & Mayer 2013).

5.2 Accretion and ULX formation

The accretion rate on to the IMBH in these captured systems has the potential to reach or even surpass the Eddington limit, resulting in the formation of an object resembling a ULX (Hopman et al. 2004). The accretion rate is primarily determined by the mass transfer rate from the companion star, which is influenced by factors such as the stellar type, orbital parameters, and the evolutionary stage of the donor star.

Hopman et al. (2004) demonstrated that the mass transfer rates in such systems can be sustained at super-Eddington levels for extended periods, potentially offering an explanation for the observed luminosities of ULXs. Subsequent studies have built upon this work, incorporating the effects of disc winds (Poutanen et al. 2007) and investigating the parameter space that allows for stable mass transfer (Fragos & McClintock 2015).

5.3 Observational implications

The formation of accreting IMBHs within mAGN discs could give rise to several observable consequences:

(1) **X-ray emission:** These systems are expected to generate X-ray emission, potentially detectable as point sources within GCs or contributing to the overall X-ray luminosity of the cluster (Maccarone et al. 2007).

(2) **Optical signatures:** The accretion disc and the irradiated companion star could produce detectable optical emission, particularly in nearby clusters (Patruno et al. 2006).

(3) **Transient phenomena:** Fluctuations in the accretion rate could lead to transient behaviour, including state transitions and outbursts (Kaaret et al. 2017).

The detection of such accreting IMBHs within GCs would provide compelling evidence for the existence of IMBHs and lend support to the mAGN scenario proposed in this study. However, differentiating these sources from other types of X-ray binaries may necessitate high-resolution X-ray observations and multiwavelength follow-up investigations.

6 LARGE-SCALE JETS FROM GAS-EMBEDDED IMBHS IN GCS

The presence of gas-embedded IMBHs in GCs raises the intriguing possibility of observable large-scale jets. While jets are commonly associated with AGNs powered by SMBHs, recent studies suggest that IMBHs might also be capable of launching significant outflows under certain conditions.

6.1 Jet formation mechanism

The formation of jets from accreting BHs is generally attributed to the interaction between the accretion disc's magnetic field and the spinning BH, as described by the Blandford–Znajek mechanism (Blandford & Znajek 1977). For IMBHs in GCs, the key requirements for jet formation would be sufficient gas supply for accretion, the presence of a magnetic field in the accretion disc, and rotation of the IMBH.

Maccarone (2004) proposed that IMBHs in GCs could indeed produce radio jets, albeit at lower luminosities compared to AGN jets. The expected radio luminosity would scale with the BH mass and accretion rate, following the fundamental plane of BH activity (Merloni, Heinz & di Matteo 2003).

The typical power of such a jet could be estimated by

$$P_{\rm jet} \approx \epsilon \dot{M}_{\rm acc} c^2 \approx 10^{42} \frac{\rm erg}{\rm s}, \tag{26}$$

where ϵ is the efficiency factor of accretion taken to be 0.1, $\dot{M}_{\rm acc}$ is the rate of mass accretion on the IMBH, and c is the speed of light. Accretion at the Eddington rate could be estimated by

$$\dot{M}_{\rm acc} = \frac{L_{\rm Edd}}{\eta c^2}, \tag{27}$$

where η is an efficiency factor, taken to be 0.1.

The Eddington luminosity is given by

$$L_{\rm Edd} = \frac{4\pi G M_{\rm IMBH} m_{\rm p} c}{\sigma_{\rm T}} \approx 10^{42} \frac{\rm erg}{\rm s} \left(\frac{M_{\rm IMBH}}{10^4\ {\rm M}_\odot} \right), \tag{28}$$

where $m_{\rm p}$ is the proton mass and $\sigma_{\rm T}$ is the Thompson scattering cross-section for electrons.

6.2 Observational prospects

Detecting jets from IMBHs in GCs presents several challenges:

(i) **Low luminosity:** The relatively low mass of IMBHs compared to SMBHs translates to less powerful jets.

(ii) **Intermittent activity:** The limited gas supply in GCs could lead to episodic accretion and jet formation, making detection more difficult.

(iii) **Resolution:** High angular resolution is necessary to resolve jets on the scale of GCs.

Despite these challenges, Mezcua (2018) suggested that deep radio observations with current and future facilities, such as the Square Kilometre Array and next-generation Very Large Array, could potentially enable the detection of jets from IMBHs in the mass range of 10^3–10^5 $M_\odot$.

6.3 Implications and future prospects

The detection of large-scale jets from gas-embedded IMBHs in GCs would have profound implications:

(i) It would provide compelling evidence for the existence of IMBHs within GCs.

(ii) It would confirm the presence of accretion discs around these IMBHs.

(iii) It would offer valuable insights into the scaling of jet properties across a vast range of BH masses.

(iv) It could potentially contribute to explaining the observed multiple stellar populations in GCs, as jets might influence the cluster's gas dynamics and star formation history (Krause et al. 2013).

Future multiwavelength observations, combining radio, X-ray, and possibly gamma-ray data, will be essential in the search for and characterization of jets from IMBHs in GCs. Such discoveries would open a new window into the physics of IMBHs and their impact on the evolution of GCs.

7 DISCUSSION

7.1 Few-body dynamics

The presence of gas within an mAGN can potentially induce binary formation (Tagawa et al. 2020; Rozner et al. 2023; Dodici & Tremaine 2024; Whitehead et al. 2024a). This process occurs when an object penetrates the Hill sphere of another object and dissipates enough energy through GDF to become gravitationally bound, forming a new binary.

For a solar-mass star orbiting an IMBH of $10^4 M_\odot$ within a disc of 10^3 au radius, the typical Hill radius is approximately 30 au. Assuming a stellar number density of $n_\star \sim 10^3$ pc^{-3} and a velocity dispersion of $\sigma \sim 10$ km s^{-1}, the capture rate into the disc is estimated to be $n R_{\rm Hill}^2 \sigma \sim 2 \times 10^{-5}$ Myr^{-1}, indicating that such captures are relatively infrequent.

Nevertheless, captures into the mAGN could potentially lead to interactions between stars within the disc, in addition to the previously discussed phenomena. These interactions might include binary-single encounters (Hut 1983; Hut & Bahcall 1983; Samsing, MacLeod & Ramirez-Ruiz 2014; Stone & Leigh 2019; Ginat & Perets 2021; Samsing et al. 2022; Trani, Quaini & Colpi 2024) or dynamical events involving higher order hierarchies. Furthermore, gas-assisted binary formation could also be triggered in principle (Rozner et al. 2023).

7.2 Survival of mAGN discs

The processes described earlier could be disrupted by the ejection of the IMBH or the destabilization of the disc.

Two primary channels could lead to IMBH ejection: recoil kicks from BH mergers and strong gravitational scatterings. Anisotropic GW emissions from BH mergers can impart high-speed kicks to IMBHs, potentially reaching velocities of $\sim 4 \times 10^3$ km s^{-1} (Merritt et al. 2004), and potentially breaking the disc after one merger. Given that the characteristic velocity dispersion in gas-free GCs is roughly 50 km s^{-1}, a significant fraction of IMBHs is expected to be ejected from the cluster, with the exact fraction depending on the mass ratio (Atallah et al. 2023).

The typical lifetime of the disc is influenced not only by the gas accretion rate but also by the capture of objects. The disc's stability is compromised once it captures a comparable mass of objects, establishing an upper limit on its lifetime.

7.3 Brownian motion

The motion of IMBHs in GCs could be described as a random walk in the momentum space, as its motion is perturbed by gravitational encounters with other celestial objects, similar to other dense environments (Merritt, Berczik & Laun 2007; Di Cintio et al. 2023).

The velocity amplitude is given by

$$\sigma_{\rm IMBH} \approx 0.07 \frac{\rm km}{\rm s} \left(\frac{\sigma_\star}{10\ {\rm km\,s^{-1}}}\right) \left(\frac{m_\star}{0.5\ {\rm M_\odot}} \frac{10^4\ {\rm M_\odot}}{M_{\rm IMBH}}\right)^{1/2}, \quad (29)$$

where $\sigma_\star$ and $m_\star$ are the velocity dispersion and mass of the background stars and $M_{\rm IMBH}$ is the mass of the IMBH.

The amplitude of the Brownian motion can be estimated by

$$\langle x^2 \rangle \approx 2Dt \approx 2\frac{\sigma^2_{\rm IMBH}}{t_{\rm coll}} t \approx 10^{-3}\ {\rm au} \frac{t}{1\ {\rm Myr}}, \quad (30)$$

where D is the diffusion coefficient of the motion, and $t_{\rm coll}$ is the typical collision time given by

$$t_{\rm coll} = \frac{1}{n\sigma_\star \pi R_\star^2} \approx 6340\ {\rm yr}, \quad (31)$$

when we considered $\sigma_\star = 10$ km s^{-1} and $R_\star = {\rm R_\odot}$. Hence, the overall displacement is not expected to significantly change the location of the IMBH and its accretion disc.

7.4 Observational implications of mAGNs

The existence of mAGNs within GCs opens up a new avenue for observational exploration and offers unique opportunities to test our understanding of IMBHs and their interaction with their environment. Indeed, there might have already been some potential indications for such phenomena (e.g. Filippenko & Ho 2003).

7.4.1 Electromagnetic signatures

The accretion process on to the IMBH within the mAGN disc is expected to produce luminous electromagnetic emission across a wide range of wavelengths. X-ray observations could reveal the presence of the mAGN through its characteristic thermal emission and potential variability (Maccarone et al. 2007). Additionally, radio observations could unveil the presence of jets emanating from the mAGN, providing further evidence of accretion on to the IMBH (Mezcua 2018). The detection of these electromagnetic counterparts would not only confirm the existence of mAGNs but also offer valuable insights into the accretion physics of IMBHs.

7.4.2 Gravitational wave signals

The dynamical processes occurring within mAGNs, such as the inspiral and merger of SBHs and IMRIs with the central IMBH, are expected to generate GWs detectable by current and future GW observatories. The detection of IMRIs and EMRIs with unique mass ratios, as discussed in Section 4.3, would offer a direct probe of IMBH demographics and their formation channels. The observation of GWs from the disruption of stars by the IMBH, or mTDEs, as outlined in Section 4.4, could shed light on the tidal disruption process and the properties of the disrupted star.

7.4.3 Unique transients

The capture and disruption of stars by the IMBH within the mAGN disc could give rise to various transient phenomena, such as mTDEs and cTDEs (see Section 4.4). These events, characterized by sudden bursts of electromagnetic radiation, could provide additional evidence of the presence of IMBHs in GCs. The study of these transients would allow us to probe the properties of the disrupted star and the accretion physics of the IMBH.

7.4.4 Variability

The interaction of stars and binaries with the mAGN disc could lead to variability in the disc's structure and accretion rate, resulting in observable variations in the electromagnetic emission from the mAGN. Monitoring the variability of mAGNs could provide valuable information about the dynamics of stars within the disc and the accretion process on to the IMBH, complementing the studies of gas hardening presented in Section 4.1.

7.4.5 Additional observational aspects

As mAGNs are expected to form mostly during the early gas-rich phases of GCs, it would be interesting to search for them in young massive clusters, which are believed to be the progenitors of GCs. Detecting mAGNs in these environments would provide crucial insights into the early evolution of IMBHs and their host clusters. Combining observations across different wavelengths, such as X-ray, radio, and optical, would offer a comprehensive view of mAGNs and their diverse observational signatures. This would enable a more detailed characterization of the accretion process, the dynamics of stars within the disc, and the potential feedback effects on the host cluster, as hinted at in Section 7.1.

8 CAVEATS AND FUTURE DIRECTIONS

Here, we briefly mention some of the possible caveats of our work:

(i) While the existence of second-generation stars in GCs is commonly observed, their formation scenario and the associated gas lifetime, amounts, and distributions remain highly uncertain. In this study, we operated under the assumption that there was at least the amount of gas required to form the second generation. However, alternative channels have been proposed to explain their existence. It is worth noting that our model could be inverted to constrain the gas content in GCs during these epochs. However, we should note that our study is also relevant for nuclear clusters hosting IMBHs, known to exist. In such galactic nuclei, multiple star formation epoch is expected from infall of gas from larger scales. In our Galaxy, Ω-Cen is thought to be the nucleus of a past dwarf galaxy, and indeed shows

evidence for clear multiple generations of star formation epochs (Woolley 1966).

(ii) The dynamics of objects embedded in gas are complex and can be modelled using various approaches and techniques, which often yield differing results. Here, we employed disc migration (Section 3.1) and GDF (Section 3.2), but other models could potentially modify our findings.

(iii) Our model necessitates the presence of an IMBH residing within a GC. Although this scenario is plausible and widely discussed in the literature, direct and conclusive evidence remains elusive. Future observations and theoretical advancements might challenge or even rule out this possibility.

(iv) The lifetime and stability of the disc are influenced by a multitude of coupled and complex processes that involve the overall evolution of the cluster. These processes could lead to a shorter disc lifetime than our predictions. The disc itself could be disrupted by violent interactions with other stars.

(v) The coalescence of objects within the disc could trigger explosive events that might prematurely disrupt the disc. However, these events could also leave behind unique observational signatures.

(vi) Global effects within the cluster could result in the segregation of stars and gas towards the centre, potentially leading to feedback mechanisms that are not considered in our current model.

(vii) Our primary focus was on gas-enriched clusters resulting from the gas associated with the second generation of star formation. As discussed earlier, other physical processes, such as accretion from the interstellar medium, could also enrich clusters with gas.

(viii) Interactions with other stars could modify the inspiral, in the case of inspiral that takes longer than the relaxation time of the cluster, e.g. in the case of disc-migration-dominated evolution.

(ix) Winds or irradiation originating from the mAGN could affect the gas in the cluster, and potentially lead to its depletion or even unbinding.

9 SUMMARY

This study explores the formation and dynamical implications of mAGNs – accretion discs around IMBHs within gas-rich GCs. We investigate conditions for stable mAGN disc formation and model the gas-induced migration of stars and BHs within them, emphasizing the dominant role of GDF.

The presence of mAGN discs could lead to several observable effects. These include alignment of stellar orbits, enhanced GW mergers with a potential frequency shift, unique TDEs (mTDEs/cTDEs), and the formation of accreting IMBH systems possibly associated with ULXs. We estimate merger rates and the various types of TDE rates, highlighting potential observational signatures.

While our study reveals intriguing possibilities, we acknowledge uncertainties related to gas properties in young GCs, complex gas dynamics, and the lack of direct IMBH observations. Nevertheless, this work underscores the importance of mAGNs in understanding IMBHs, GC evolution, and potentially the formation of SMBHs. Future multiwavelength observations are crucial for confirming their existence and characterizing their properties.

ACKNOWLEDGEMENTS

We would like to thank Evgeni Grishin for fruitful discussions, and Barry Ginat for fruitful discussions and a tea tray. MR acknowledges the generous support of Azrieli & Rothschild fellowships. AAT acknowledges support from the Horizon Europe research and innovation programmes under the Marie Skłodowska-Curie grant agreement no. 101103134.

DATA AVAILABILITY

The data underlying this article will be shared on reasonable request to the corresponding author.

REFERENCES

Abbott B. P. et al., 2017, Phys. Rev. D, 96, 022001
Abbott B. P. et al., 2019, Phys. Rev. D, 100, 064064
Abbott R. et al., 2020, ApJ, 900, L13
Abbott R. et al., 2022, A&A, 659, A84
Amaro-Seoane P., 2018, Living Rev. Relativ., 21, 4
Amaro Seoane P., 2022, in Bambi C., Katsanevas S., Kokkotas K. D., eds, Handbook of Gravitational Wave Astronomy. Springer, Singapore, p. 17
Amaro-Seoane P., Gair J. R., Freitag M., Miller M. C., Mandel I., Cutler C. J., Babak S., 2007, Class. Quantum Gravity, 24, R113
Antoni A., MacLeod M., Ramirez-Ruiz E., 2019, ApJ, 884, 22
Artymowicz P., Lin D. N. C., Wampler E. J., 1993, ApJ, 409, 592
Atallah D., Trani A. A., Kremer K., Weatherford N. C., Fragione G., Spera M., Rasio F. A., 2023, MNRAS, 523, 4227
Bartos I., Kocsis B., Haiman Z., Márka S., 2017, ApJ, 835, 165
Bastian N., Lardo C., 2015, MNRAS, 453, 357
Begelman M. C., Volonteri M., Rees M. J., 2006, MNRAS, 370, 289
Blandford R. D., Znajek R. L., 1977, MNRAS, 179, 433
Cantiello M., Jermyn A. S., Lin D. N. C., 2021, ApJ, 910, 94
Di Cintio P., Pasquato M., Barbieri L., Trani A. A., di Carlo U. N., 2023, A&A, 673, A8
Dodici M., Tremaine S., 2024, ApJ, 972, 193
Duffell P. C., Haiman Z., MacFadyen A. I., D'Orazio D. J., Farris B. D., 2014, ApJ, 792, L10
Duffell P. C., D'Orazio D., Derdzinski A., Haiman Z., MacFadyen A., Rosen A. L., Zrake J., 2020, ApJ, 901, 25
Eardley D. M., Press W. H., 1975, ARA&A, 13, 381
Ebisuzaki T. et al., 2001, ApJ, 562, L19
Fabj G., Nasim S. S., Caban F., Ford K. E. S., McKernan B., Bellovary J. M., 2020, MNRAS, 499, 2608
Filippenko A. V., Ho L. C., 2003, ApJ, 588, L13
Fragione G., 2022, ApJ, 939, 97
Fragione G., Leigh N., 2018, MNRAS, 480, 5160
Fragione G., Leigh N. W. C., Ginsburg I., Kocsis B., 2018, ApJ, 867, 119
Fragos T., McClintock J. E., 2015, ApJ, 800, 17
Fujii M. S., Wang L., Tanikawa A., Hirai Y., Saitoh T. R., 2024, Science, 384, 1488
Gangardt D., Trani A. A., Bonnerot C., Gerosa D., 2024, MNRAS, 530, 3689
Generozov A., Perets H. B., 2023, MNRAS, 522, 1763
Ginat Y. B., Perets H. B., 2021, Phys. Rev. X, 11, 031020
Ginat Y. B., Panamarev T., Kocsis B., Perets H. B., 2023, MNRAS, 525, 4202
Grishin E., Perets H. B., 2016, ApJ, 820, 106
Grishin E., Bobrick A., Hirai R., Mandel I., Perets H. B., 2021, MNRAS, 507, 156
Grishin E., Gilbaum S., Stone N. C., 2024, MNRAS, 530, 2114
Gualandris A., Merritt D., 2009, ApJ, 705, 361
Haiman Z., Kocsis B., Menou K., 2009, ApJ, 700, 1952
Hendriks K., Zwick L., Samsing J., 2024, preprint (arXiv:2408.04603)
Hopman C., Alexander T., 2005, ApJ, 629, 362
Hopman C., Portegies Zwart S. F., Alexander T., 2004, ApJ, 604, L101
Hut P., 1983, ApJ, 268, 342
Hut P., Bahcall J. N., 1983, ApJ, 268, 319
Ida S., Lin D. N. C., 2004, ApJ, 616, 567
Kaaret P., Feng H., Roberts T. P., 2017, ARA&A, 55, 303
Kanagawa K. D., Tanaka H., Szuszkiewicz E., 2018, ApJ, 861, 140
Krause M., Charbonnel C., Decressin T., Meynet G., Prantzos N., 2013, A&A, 552, A121
Kritos K., Cholis I., 2020, Phys. Rev. D, 102, 083016

Kroupa P., 2002, Science, 295, 82
Leigh N. W. C., Böker T., Maccarone T. J., Perets H. B., 2013, MNRAS, 429, 2997
Leigh N. W. C., Mastrobuono-Battisti A., Perets H. B., Böker T., 2014, MNRAS, 441, 919
Levin Y., 2007, MNRAS, 374, 515
Li R., Lai D., 2022, MNRAS, 517, 1602
Li R., Lai D., 2023a, MNRAS, 522, 1881
Li J., Lai D., 2023b, ApJ, 956, 17
Li J., Dempsey A. M., Li H., Lai D., Li S., 2023, ApJ, 944, L42
Lin D. N. C., Murray S. D., 2007, ApJ, 661, 779
Lin D. N. C., Papaloizou J., 1979a, MNRAS, 186, 799
Lin D. N. C., Papaloizou J., 1979b, MNRAS, 188, 191
Lin D. N. C., Papaloizou J., 1986, ApJ, 309, 846
Maccarone T. J., 2004, MNRAS, 351, 1049
Maccarone T. J., Kundu A., Zepf S. E., Rhode K. L., 2007, Nature, 445, 183
McKernan B., Ford K. E. S., Lyra W., Perets H. B., 2012, MNRAS, 425, 460
MacLeod M., Trenti M., Ramirez-Ruiz E., 2016, ApJ, 819, 70
Madau P., Rees M. J., 2001, ApJ, 551, L27
Mandel I., Brown D. A., Gair J. R., Miller M. C., 2008, ApJ, 681, 1431
Mapelli M., Zampieri L., Mayer L., 2013, MNRAS, 429, 2298
Mastrobuono-Battisti A., Perets H. B., 2013, ApJ, 779, 85
Merloni A., Heinz S., di Matteo T., 2003, MNRAS, 345, 1057
Merritt D., Milosavljević M., Favata M., Hughes S. A., Holz D. E., 2004, ApJ, 607, L9
Merritt D., Berczik P., Laun F., 2007, AJ, 133, 553
Mezcua M., 2018, Int. J. Mod. Phys. D, 27, 1830021
Miller M. C., Freitag M., Hamilton D. P., Lauburg V. M., 2005, ApJ, 631, L117
Mishra B., Calcino J., 2024, preprint (arXiv:2409.05614)
Moody M. S. L., Shi J.-M., Stone J. M., 2019, ApJ, 875, 66
Muñoz D. J., Lai D., Kratter K., Miranda R., 2020, ApJ, 889, 114
Murray C. D., Dermott S. F., 2000, Solar System Dynamics. Cambridge University press
Naiman J. P., Ramirez-Ruiz E., Lin D. N. C., 2011, ApJ, 735, 25
Nasim S. S. et al., 2023, MNRAS, 522, 5393
O'Neill D., D'Orazio D. J., Samsing J., Pessah M. E., 2024, ApJ, 974, 216
Ostriker J. P., 1983, ApJ, 273, 99
Ostriker E. C., 1999, ApJ, 513, 252
Paardekooper S. J., Baruteau C., Crida A., Kley W., 2010, MNRAS, 401, 1950
Panamarev T., Shukirgaliyev B., Meiron Y., Berczik P., Just A., Spurzem R., Omarov C., Vilkoviskij E., 2018, MNRAS, 476, 4224
Patruno A., Portegies Zwart S., Dewi J., Hopman C., 2006, MNRAS, 370, L6
Perets H. B., 2022, ApJ, 927, L23
Perets H. B., Li Z., Lombardi J. C.,, Jr Milcarek S. R.,, Jr 2016, ApJ, 823, 113
Peterson B. M. et al., 2005, ApJ, 632, 799
Portegies Zwart S. F., McMillan S. L. W., 2002, ApJ, 576, 899
Poutanen J., Lipunova G., Fabrika S., Butkevich A. G., Abolmasov P., 2007, MNRAS, 377, 1187
Raveh Y., Perets H. B., 2021, MNRAS, 501, 5012
Rees M. J., 1988, Nature, 333, 523
Rein H., 2012, MNRAS, 422, 3611
Rose S. C., Naoz S., Sari R., Linial I., 2022, ApJ, 929, L22
Rowan C., Boekholt T., Kocsis B., Haiman Z., 2023, MNRAS, 524, 2770
Rowan C., Whitehead H., Boekholt T., Kocsis B., Haiman Z., 2024, MNRAS, 527, 10448
Rozner M., Perets H. B., 2022, ApJ, 931, 149
Rozner M., Generozov A., Perets H. B., 2023, MNRAS, 521, 866
Safronov V. S., 1960, Ann. Astrophys., 23, 979
Samsing J., MacLeod M., Ramirez-Ruiz E., 2014, ApJ, 784, 71
Samsing J. et al., 2022, Nature, 603, 237
Samsing J., Hendriks K., Zwick L., D'Orazio D. J., Liu B., 2024, preprint (arXiv:2403.05625)
Shakura N. I., Sunyaev R. A., 1973, A&A, 24, 337
Sigurdsson S., Hernquist L., 1993, Nature, 364, 423
Silk J., 2017, ApJ, 839, L13
Sirko E., Goodman J., 2003, MNRAS, 341, 501
Stone N. C., Leigh N. W. C., 2019, Nature, 576, 406
Stone N. C., Metzger B. D., Haiman Z., 2017, MNRAS, 464, 946
Tagawa H., Haiman Z., Kocsis B., 2020, ApJ, 898, 25
Tanaka T., 2008, J. Phys.: Conf. Ser., 120, 032001
Tanaka H., Takeuchi T., Ward W. R., 2002, ApJ, 565, 1257
Tang V. L., Madau P., Bortolas E., Peng E. W., Feng Y., Guhathakurta P., 2024, ApJ, 963, 146
Toomre A., 1964, ApJ, 139, 1217
Trani A. A., Quaini S., Colpi M., 2024, A&A, 683, A135
Vaccaro M. P., Mapelli M., Périgois C., Barone D., Artale M. C., Dall'Amico M., Iorio G., Torniamenti S., 2024, A&A, 685, A51
van de Ven G., van den Bosch R. C. E., Verolme E. K., de Zeeuw P. T., 2006, A&A, 445, 513
Ward W. R., 1997, Icarus, 126, 261
Whitehead H., Rowan C., Boekholt T., Kocsis B., 2024a, MNRAS, 531, 4656
Whitehead H., Rowan C., Boekholt T., Kocsis B., 2024b, MNRAS, 533, 1766
Woolley R. V. D. R., 1966, R. Obs. Ann., 2, 1

This paper has been typeset from a TEX/LATEX file prepared by the author.